Transfer Learning for Neuroimaging via Re-use of Deep Neural Network Features

Peter Holderrieth[1,3], Han Peng[2], and Stephen Smith[3]

[1]Department of Physiology, Anatomy, and Genetics, University of Oxford
[2]Visual Geometry Group (VGG), University of Oxford, Oxford, United Kingdom
[3]FMRIB Centre, Wellcome Centre for Integrative Neuroimaging (WIN), Nuffield Department of Clinical Neurosciences, University of Oxford, Oxford, United Kingdom

December 12, 2022

Abstract. A major problem in the application of machine learning to neuroimaging is the technological variability in the MRI scanners and the different subject populations across studies. Transfer learning (TL) promises to alleviate this problem. TL refers to a family of methods which acquire knowledge from related tasks to improve generalization in the tasks of interest. In this work, we show that features of deep neural networks are transferable across data sets if the network was pre-trained on the prediction task of interest. Based on this, we propose a transfer learning pipeline which relies on the re-use of deep neural network features across data sets. We empirically study this pipeline on age and sex prediction using the UK Biobank for pre-training and three different small data sets for fine-tuning and evaluation. We find that our method outperforms classical regression methods and training a network from scratch. In particular, we improve state-of-the-art results on age and sex prediction. Our transfer learning method may therefore provide a simple and efficient pipeline to achieve high performance on small data sets.

Contents

List of Figures **3**

List of Tables **4**

1 Introduction **5**

2 Methods **7**
2.1 Deep Learning 7
2.2 Data 11
2.3 Elastic net regression 14

3 Results **15**
3.1 Transfering deep neural networks across MRI scanners 15
3.2 Transfer learning vs. classical regression methods 20
3.3 Comparing results to other works 20
3.4 Explaining the performance gain of transfer learning 22
3.5 Transfer learning and data scarcity 23
3.6 Convergence time 24

4 Discussion **26**
4.1 Pre-training on large data sets 26
4.2 Traditional machine learning vs. deep learning 26
4.3 Transfer learning vs. training from scratch 27
4.4 Comparison with other transfer learning approaches 27

5 Conclusion **30**

List of Figures

2.1 Illustration of SFCNs 8
2.2 Illustration of data augmentation 9
2.3 MRI scan examples from different data sets 12

3.1 Plotting SFCN features of UKB via t-SNE 16
3.2 Illustration of t-SNE plot with ”brain manifold” 17
3.3 Plotting SFCN features after domain shift 18
3.4 Plotting SFCN features after fine-tuning the feature extractor 21
3.5 Studying performance depending on the size of the training set 23
3.6 Comparing training convergence between randomly initialized models and transfer learning 24

List of Tables

2.1 Summary statistics of data sets 13
2.2 Technical details in data acquisition 14

3.1 Testing SFCNs pre-trained on UKB on different data sets 15
3.2 Fine-tuning classifier of SFCNs pre-trained on different tasks 19
3.3 Comparing results between fine-tuning only the final layer and algorithm 1 . . . 20
3.4 Regression vs. transfer learning 22
3.5 Random initialization vs. transfer learning 23

1 Introduction

With the availability of big labeled data sets such as ImageNet [1], the application of deep neural networks [2] has shown huge success in a variety of fields such as computer vision, natural language processing [3] or speech [4]. In biomedical imaging, deep learning led to advances in areas such as automated diagnostics [5, 6, 7] or image segmentation [8] showing the huge potential of the application of artifical intelligence (AI) in healthcare [9]. In neuroimaging, the benefit of deep learning remains a subject of debate with some works showing that classical regression methods are not outperformed by deep learning techniques [10, 11, 12, 13, 14].

One challenge for applying deep learning in neuroimaging is that brain scans are usually expensive to acquire, which causes data sets to be small. On top of that, one faces the problem that there are significant differences in the image statistics across data sets, a phenomenon called domain shift (DS). In neuroimaging, this can be caused by technical differences [15] in imaging protocols, image resolution, contrast, signal-to-noise ratio or MRI hardware (e.g. MRI scanners at different hospitals). Moreover, DS occurs if different studies have different subject populations such as demographics or disease prevalence [16]. DS causes machine learning models which are trained for a task in one dataset to perform significantly worse when applied to the same task in another dataset [17].

One approach to solve this is called *transfer learning* (TL). TL is a set of machine learning methods that enable to acquire knowledge from related tasks to improve performance on the task of interest - the *target task*. A doctor specialized in computed tomography (CT) could learn how to analyze MRI images much faster than someone with no background in radiology. TL tries to mimic such a transfer of knowledge on a machine learning level.

In this work, we try to solve the problem of DS in neuroimaging by the efficient re-use of features of deep neural networks across data sets. In computer vision, it is common practice to pre-train models in a large natural image dataset (e.g. ImageNet) and then finetune the models in the target small datasets to achieve faster convergence and better performance [18]. Yet, while several successful applications of deep learning in medicine such as skin cancer classification or detection of diabetic retinopathy follow this pipeline [19, 20], other works question the benefit of such procedures in medical imaging [21].

In the last years, big brain imaging datasets such as the UK Biobank (UKB) and the Human Connectome Project (HCP) have become available opening new opportunities for harnessing the power of such data sets [22, 23]. Recently, these also showed to enable highly accurate machine learning in the neuroimaging domain. For example, Peng et al. [24] showed by proposing a light-weight deep neural network for 3d brain images that deep learning can outperform tradi-

tional machine learning techniques in brain age and sex prediction on data from the UKB. Here, we built on this work studying whether we can achieve high performance even for small data sets via transfer learning and whether a big neuroimaging data set such as the UKB can help alleviate the problem of DS. To test our method, we use the three data sets from other studies: the OASIS-3 [25], ABIDE (I and II) [26] and IXI [27] data sets.

We focus our attention on age and sex prediction based on structual MRI data as age and sex are labels which are available across all data sets. Predicting sex and age also serve as non-trivial surrogate tasks sharing challenges with tasks such as disease prediction. In addition, the prediction of age based on clinical MRI data is also clinically relevant as the difference between the predicted age and the actual age, i.e. the brain age delta, can serve as an effective biomarker [28], e.g. for prediciting mortality [29].

We make the following contributions:

1. We systematically study the re-use of features of deep neural networks across scanners and show that features are re-usable even if DS occurs.

2. We propose an easy-to-use and effective transfer learning method to alleviate the problem of DS.

3. We show that via transfer learning, deep neural networks achieve significantly stronger performance than classical regression methods even in the small data regime. In addition, our results improve state-of-the-art on age and sex prediction.

4. We show that the superior performance can be attributed to the re-use of features learnt on the pre-training data set.

This document is structured as follows. In chapter 2, the machine learning methods and data sets which we use are described in more detail. In chapter 3, we study the re-use of deep neural network features from where we derive our method and present experimental results. In chapter 4, we relate our results with previous works and discuss future directions.

2 Methods

2.1 Deep Learning

We begin by discussing the deep learning methods we use.

2.1.1 Simple Fully Connected Neural Networks (SFCNs)

As a deep learning model, we use Simple Fully Connected Neural Networks (SFCNs) which were introduced by Peng et al. [24]. SFCNs built on the idea of fully convolutional neural networks [30]. Using almost exclusively convolutional layers as opposed to dense layers, the number of parameters of the deep neural network is drastically reduced allowing to build networks with many layers - even for the memory-intensive 3d MRI scans.

SFCNs consist of two main components: a feature extractor and a classifier (see fig. 2.1). The feature extractor receives a 3d MRI scan as input and outputs a high-dimensional vector. We interpret this as a *feature vector* of the scan following a common interpretation of deep neural networks [2]. Based on this feature vector, the classifier then outputs the predicted label.

The feature extractor consists of 6 blocks: each of the first 5 blocks consist of a 3d convolutional layer of kernel size 3x3x3 with subsequent batch-normalization [31], max-pooling layer of size 2x2x2 and a final Relu non-linearity. The sixth block consists of a 3d convolutional layers of kernel size 1x1x1 with subsequent batch-normalization and a Relu non-linearity.

The classifier consists of an average pooling layer, a dropout layer [32], a $1 \times 1 \times 1$ convolution, and a final softmax function giving a probability distribution $p = (p_1, \ldots, p_n)$ over n bins. If the model is trained on a classification problem, e.g. sex prediction, every bin would represent a class, e.g. female or male, and the predicted class would be the class of highest probability. If the model is trained on a regression problem such as age prediction, SFCNs frame this as a classification problems as well by assigning every bin $i = 1, \ldots, n$ a value range $[b_i, b_{i+1}]$. The predicted age $\hat{y}$ is then given by the expected value:

$$\hat{y} = \sum_{i=1}^{n} p_i \frac{b_i + b_{i+1}}{2}$$

2.1.2 Loss

To compute the loss between the output of the model, i.e. the probability distribution $p = (p_1, \ldots, p_n)$ across bins, and the true label y, we use two losses depending on the label type.

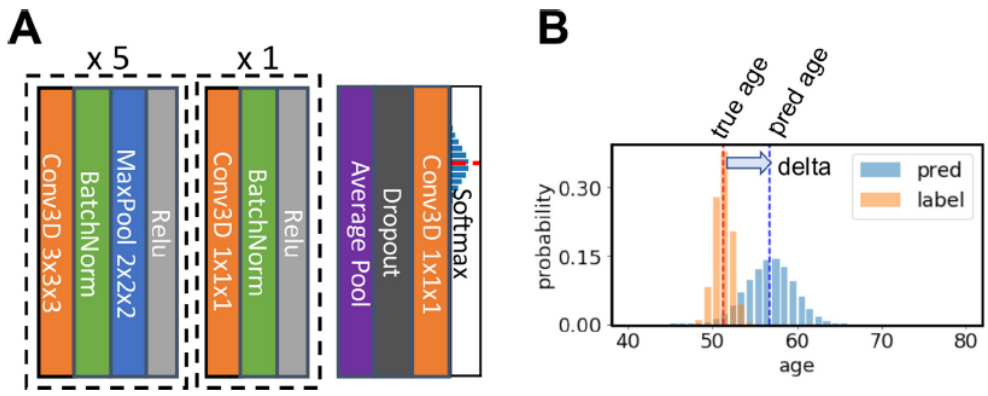

Figure 2.1: Illustration of SFCNs. **A:** the feature extractor consists of 6 blocks with convolutional layers, batchnorm, and Relu layers. The first 5 blocks have convolutions with kernel size $3 \times 3 \times 3$ and an additional max-pooling layer, while the last block has kernel size $1 \times 1 \times 1$. The classifier consists of an average pooling layer, a dropout layer, a fully connected layer, here similar to a $1 \times 1 \times 1$ convolution, and a softmax layer. **B:** the output of SFCNs is a probability distribution over the possible labels. As depicted here for age prediction, the model is trained to output a discretization of the normal distribution $\mathcal{N}(y, 1)$ where y is the true age of the subject.

For age, we assign every age label y a bin distribution $q = (q_1, q_2, \ldots, q_n)$ where q_i is the probability of bin $[b_i, b_{i+1}]$ under the normal distribution $\mathcal{N}(y, 1)$ with mean y and unit variance, i.e.

$$q_i = \int_{b_i}^{b_{i+1}} \frac{1}{\sqrt{2\pi}} \exp\left(-\frac{1}{2}(z-y)^2\right) dz$$

The loss is then the Kullback-Leibler divergence

$$L(y, p) = \mathrm{KL}(q \| p) = \sum_{i=1}^{n} q_i \log\left(\frac{q_i}{p_i}\right)$$

For sex, the model outputs a probability distribution $p = (p_f, p_m)$ where p_f (resp. p_m) is the probability for female (resp. male). We then use the cross-entropy as a loss between the true label $y \in \{f, m\}$ and the output of the model:

$$L(y, p) = -1_{y=f} \log(p_f) - 1_{y=m} \log(p_m)$$

2.1.3 Training

To train our model, we minimized the loss using Stochastic Gradient Descent (SGD). We trained our model using classical momentum of the learning rate [33]. We used a learning rate scheduler

decaying the learning rate after n epochs by a factor of $\lambda \in [0, 1]$.

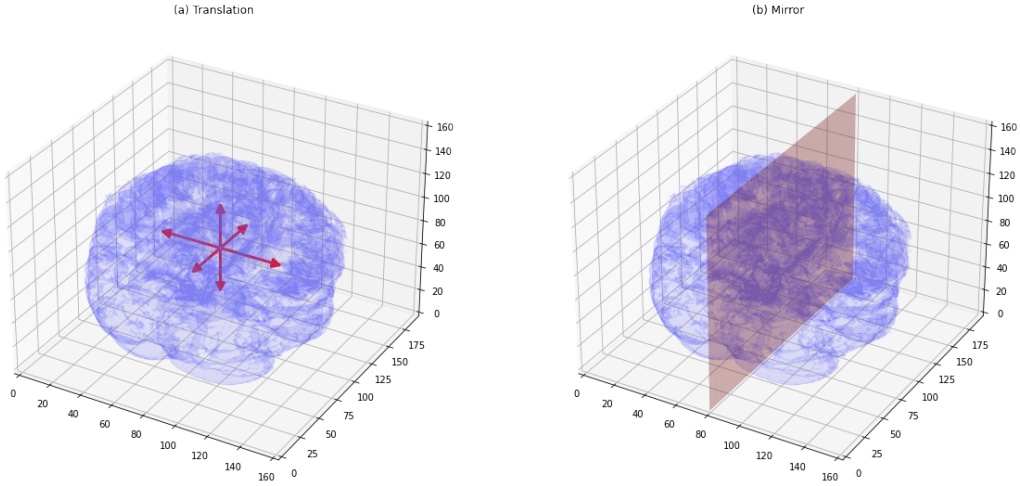

Figure 2.2: Illustration of data augmentation. (a) random translation along any of the three axis. (b) random mirroring along the sagittal plane

An MRI scan is represented by an array of voxel intensities as input and we divide the array by its own mean intensity following previous work [24]. To increase the amount of data samples, we perform data augmentation in two ways (see fig. 2.2): first, we perform a random shift along the x-,y-, and z-axis by ± 2 voxels. Second, we mirror an MRI scan with probability $p = 0.5$ along the sagittal section. This effectively increases the number of data samples by a factor of 250 and is therefore of particular importance since we target small data sets. We stress that this data augmentation is only performed during training and not during testing.

As common, we optimized the loss on the train set and optimized hyperparameters of the model on the validation set. The test set was untouched until all hyperparameters had been optimized.

2.1.4 Implementation

To perform automatic differentation, we implemented SFCNs and the training procedures with *PyTorch* [34]. The models were trained on NVIDIA GeForce GTX 1080 Ti GPUs. Usually, computations were done with 2 GPUs in parallel. The anonymized github repository with the code can be found at: *https://anonymous.4open.science/r/974dad70-0547-4ca9-998c-6781c333ae01/*.

2.1.5 Transfer Learning

In transfer learning [35], we are given two data sets which complement each other.

First, we are given a target data set $Z = \{(\mathbf{x}_i, \mathbf{y}_i)\}_{j=1}^{m}$ where $(\mathbf{x}_i, \mathbf{y}_i) \sim P$ are independent samples from a distribution P. We want our model to "learn" P. However, usually the size m of the data set is quite small. In our case, $\mathbf{x}_i$ corresponds to an MRI scan and $\mathbf{y}_i$ corresponds to age or sex.

Second, we are given a pre-training data set $Z' = \{(\mathbf{x}'_i, \mathbf{y}_i)'\}_{i=1}^{m'}$ whose size m' is usually big. However, there is a domain shift, i.e. the pairs $(\mathbf{x}'_i, \mathbf{y}'_i)$ are samples $(\mathbf{x}'_i, \mathbf{y}'_i) \sim P'$ from a distribution $P' \neq P$, e.g. due to different properties of MRI scanners. Assuming that P and P' are "similar", the idea of transfer learning is to use the abundance of data from P', i.e. the size m' of Z', to learn the task P of interest. In our case, Z' is the UKB, and Z is one of ABIDE, IXI, or OASIS.

Our transfer learning pipeline is summarized in algorithm 1. One starts to randomly initialize the parameters of a model M and trains it with the abundant data set Z'. In many cases, the output dimension, i.e. number of bins, may vary between Z and Z'. If this is the case, one first reshapes the classifier of the SFCN and re-trains the classifier keeping the feature extractor fixed. Finally, one trains the full model on the target data set Z.

To differentiate the training processes, we will use the term *pre-training* for training a randomly initialized model and the term *fine-tuning* for training a model whose parameters were loaded from a previous training process.

Algorithm 1: Transfer Learning with SFCNs

Input: Target data set $Z = \{(\mathbf{x}_i, \mathbf{y}_i)\}_{i=1}^{n}$, pre-training data set $Z' = \{(\mathbf{x}'_i, \mathbf{y}'_i)\}_{j=1}^{m}$;
Randomly initialize parameters of model M;
Train M on Z';
$d = \dim(\mathbf{y}_i)$;
$d' = \dim(\mathbf{y}'_i)$;
if $d \neq d'$ **then**
  Reshape the classifier such that output dimension is d;
  Train the classifier on Z;
end
Train M on Z;
return M

2.2 Data

2.2.1 Data sets

UKB. As a pre-training data set, we use the UK Biobank (UKB). The UKB is a collection of brain imaging data from predominantly healthy participants [22]. In this work, we used the T1-weighted MRI scans from 40000 subjects. The image pre-processing pipeline is described in [36].

OASIS. The Open Access Series of Imaging Studies 3 (OASIS-3) [25] contains 1098 subjects and 2168 longitudinal MRI scanning sessions. Following LaMontagne et al. [25], the healthy control group consists of the subjects who have CDR score 0 from all clinical visits during the longitudinal studies. Only the 3T MRI sessions with valid clinical visit (within one year since or before the MRI scan) are included. This was because OASIS-3 contains both 1.5T and 3T MRI scans, while the CNN models were pretrained in UK Biobank scans using only 3T MRI. The selection process results in 1036 eligible subjects and 1806 eligible sessions.

IXI. The IXI dataset [27] contains MR images from normal, healthy subjects. We used the 3T scans resulting in 538 available scans.

ABIDE. The Autism Brain Imaging Data Exchange (ABIDE) initiative [26] collected MR images from both neurotypical and autistic subjects. We followed the selection process by [37].

In fig. 2.3, one can see various samples of MRI scans from the different data sets.

2.2.2 Data pre-processing

The preprocessing pipeline uses the *fsl_anat* command from the FSL library [38] for automatic bias field removal, 12 degree of freedom linear registration, and non-linear registration to a standard space (2mm MNI 152 space), purely for the purpose of brain extraction. Finally, the 1mm brain is linearly transformed to MNI 152 with FLIRT [39, 40, 41] and used for the subsequent training/validation/testing for deep learning.

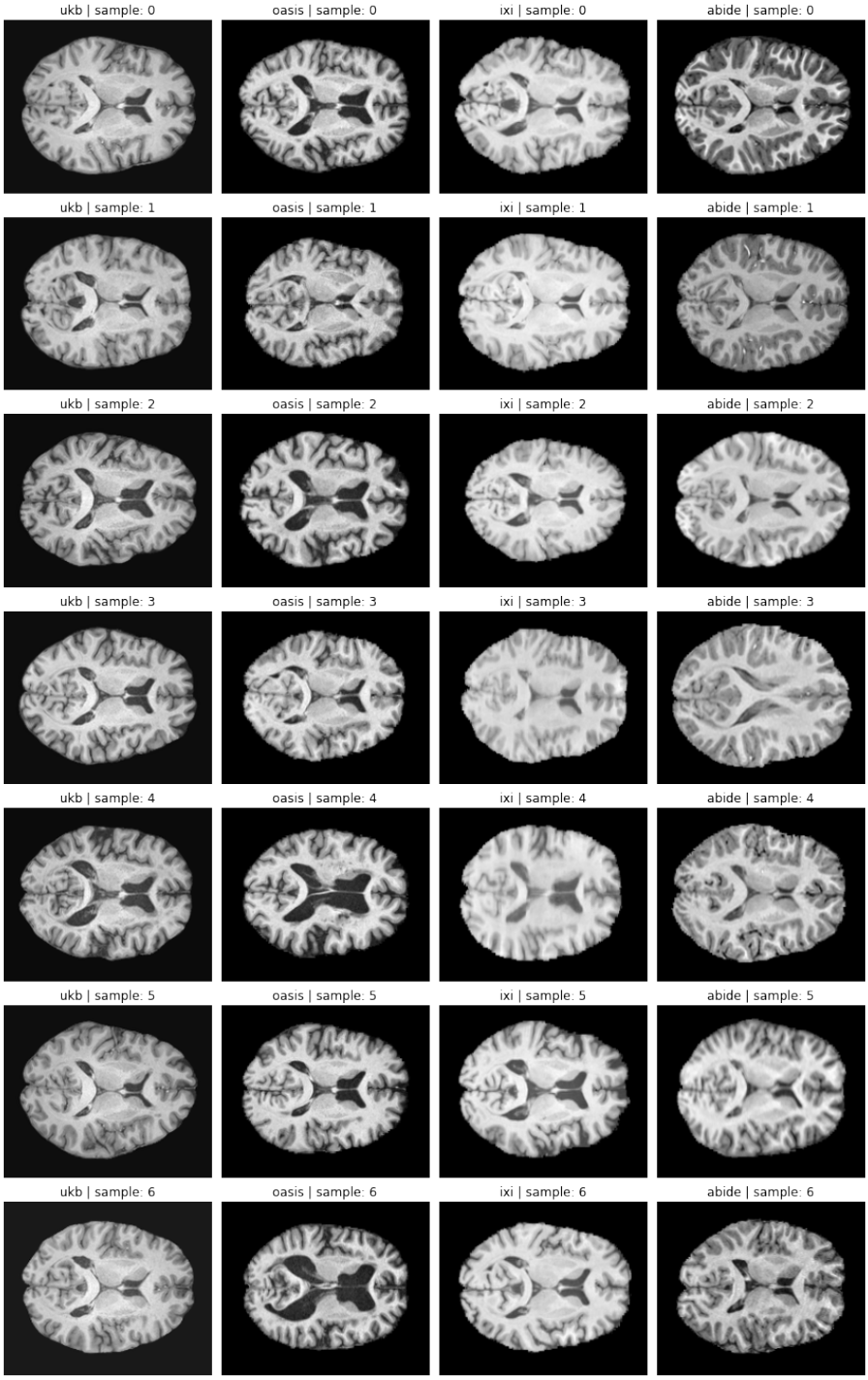

Figure 2.3: Samples of MRI scans (horizontal section). Every row gives a different sample. First column: UKB. Second: OASIS. Third: IXI. Fourth: ABIDE

2.2.3 Split of data sets

We split all data sets randomly in a train, validation, and test set (see table 2.1). The selection was done by randomly partitioning the subjects in a train, validation, and test group. For the training and validation set, we included all MRI sessions of a subject, while in the test set we only had one MRI session per subject.

In OASIS, we performed a completely random split. In IXI and ABIDE, the sampling process respected scanner site, share of females, and the age distribution ensuring a similar share per respective class in every train, validation, and test set. As one can see in table 2.1, the numbers of samples per data set is significantly smaller than the UKB and the share of females vary significantly across OASIS, IXI, and ABIDE. Moreover, the age distribution varies as well, e.g. ABIDE covers relatively young subjects of 5-55 years old while OASIS covers an old population of 42-95 years. In sum, these data sets represents a variety of realistic domain shifts in terms of subject population and serve as good examination tasks for transfer learning.

Table 2.1: Summary statistics of data sets

	OASIS			**IXI**			**ABIDE**			**UKB**
	train	valid	test	train	valid	test	train	valid	test	
n total	355	91	686	215	108	215	537	269	537	39677
n female	228	50	272	120	63	114	147	70	127	20999
n male	127	41	414	95	45	101	389	199	409	18678
age min	42.7	48.4	45.8	20.1	20.2	20.0	5.2	5.43	5.32	44.6
age max	95.2	92.1	95.7	86.2	86.3	83.5	56.2	54.0	55.4	82.3
age mean	68.6	68.8	68.9	47.7	50.7	46.5	13.6	13.6	13.2	64.1
age std	8.1	9.7	8.8	16.7	16.7	15.2	6.52	6.2	6.0	7.5

As one can see in table 2.1, the number of female and male subjects vary across data sets. If we train or test models on sex prediction, we therefore balanced the data sets by oversampling the underrepresented sex, i.e. we randomly sampled subjects from the underrepresented sex and inserted them into the data set.

On top of subject population, we would also expect a significant domain shift in terms of technical difference across scanning procedures. As one can see in table 2.2, the number of different scanner models used and the number of different scanner sites vary significantly. These differences might also explain the variations seen in fig. 2.3: OASIS and UKB seem relatively similar in contrast and brightness, while IXI seems brighter and ABIDE shows big variation in terms of brightness.

Table 2.2: Technical acquisition details about data sets

Data	**Scanner brands**	n **scanner models**	n **sites**
UKB	Siemens	1	3
OASIS	Siemens	1	2
IXI	Philips, GE	3	3
ABIDE	Philips, GE, Siemens	6	19

2.3 Elastic net regression

To perform regression on the MRI scans, we perform principal component analysis (PCA) on the train data and choose the k principal components which are most correlated with the labels (either age or sex). We then perform elastic net regression [42] on these principal components. To compute predictions based on the validation and test data, we simply project the data to the k previously selected features and perform predictions with the fitted linear regression parameters.

3 Results

3.1 Transfering deep neural networks across MRI scanners

We first study the effects of using a deep neural network for MRI scanner sites or data sets which it was not trained on. These results give a justification for our transfer learning method (see algorithm 1) and empirically show the effects of domain shift.

3.1.1 Direct transfer

We begin by studying the change in performance after domain shift. We look at sex prediction and use 5 models which were pre-trained on the UKB with different random seeds. On the UKB, we achieve very accurate results of 99.5%. However, as one can see in table 3.1, there is a significant decline in performance when testing such a model on different data sets. The high performance on OASIS might be explained by the similarities of age distribution and scanners to the UKB (see section $2.2.3$ and fig. 2.3). While performance varies significantly with accuracy of 90.2% on OASIS and 59.1% on IXI, in all data sets we observe a significantly higher performance than random selection, i.e. higher than 50%. This indicates that pre-training on UKB equips a model with an inference rule which is better than random initialization and at least partially transferable across data sets. It seems therefore sensible to re-use the information from a model even if it was trained on a different data set.

Table 3.1: Testing SFCNs pre-trained on UKB sex classification on different data sets. Mean and standard deviation over 5 runs. Data sets were balanced for sex.

Dataset	**Accuracy**
UKB	$99.5\% \pm 0.1\%$
OASIS	$90.2\% \pm 2.5\%$
ABIDE	$59.9\% \pm 4.9\%$
IXI	$59.1\% \pm 7.0\%$

3.1.2 Feature re-use and task specificity of features

We next study why such a decline in performance occurs. As explained in section $2.1.1$, SFCNs consist of a feature extractor and a classifier. We can visualize how SFCNs learn to extract information from MRI scans by visualizing the high-dimensional features produced by the feature

extractor (see figs. 3.1 and 3.2).

We use two models which were trained on the UKB. The first one was trained on age prediction and the second one was trained on sex prediction. Passing MRI scans from the UKB test set through the feature extractor of the pre-trained models, we perform dimensionality reduction on the acquired data via t-distributed stochastic neighborhood selection (t-SNE) [43] (see fig. 3.2 as an illustration). As one can see in fig. 3.1, the feature extractor spatially separates MRI scans in a ”manifold” giving a continuous spectrum of age and a distinction between female and male participants. It is particularly striking that features are highly specific to the task which the model was trained on. For example, the features from a model trained on age prediction do not spatially separate scans of female and male subjects (see fig. 3.1 (b)). It therefore seems plausible that for transfer learning, we should use models which were pre-trained on the same task.

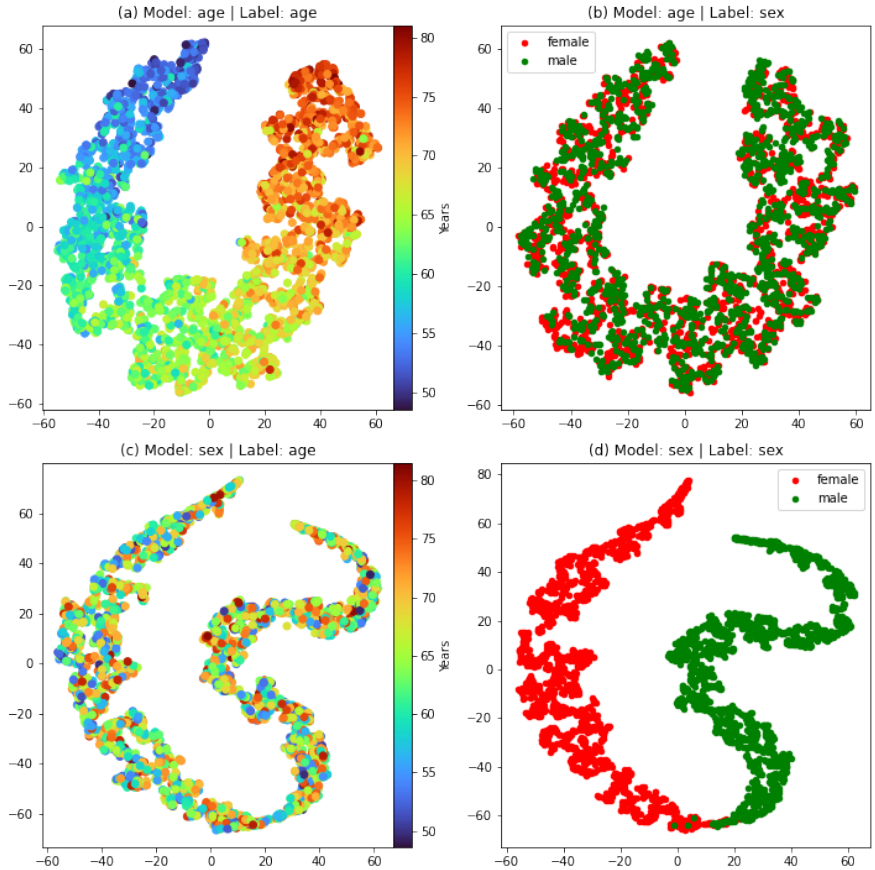

Figure 3.1: Plotting SFCN features of UKB via t-SNE. (a),(b): model trained on age. (c),(d): model trained on sex. One can observe that a model trained on age does not spatially differentiate sex and a model trained on sex does not separate age.

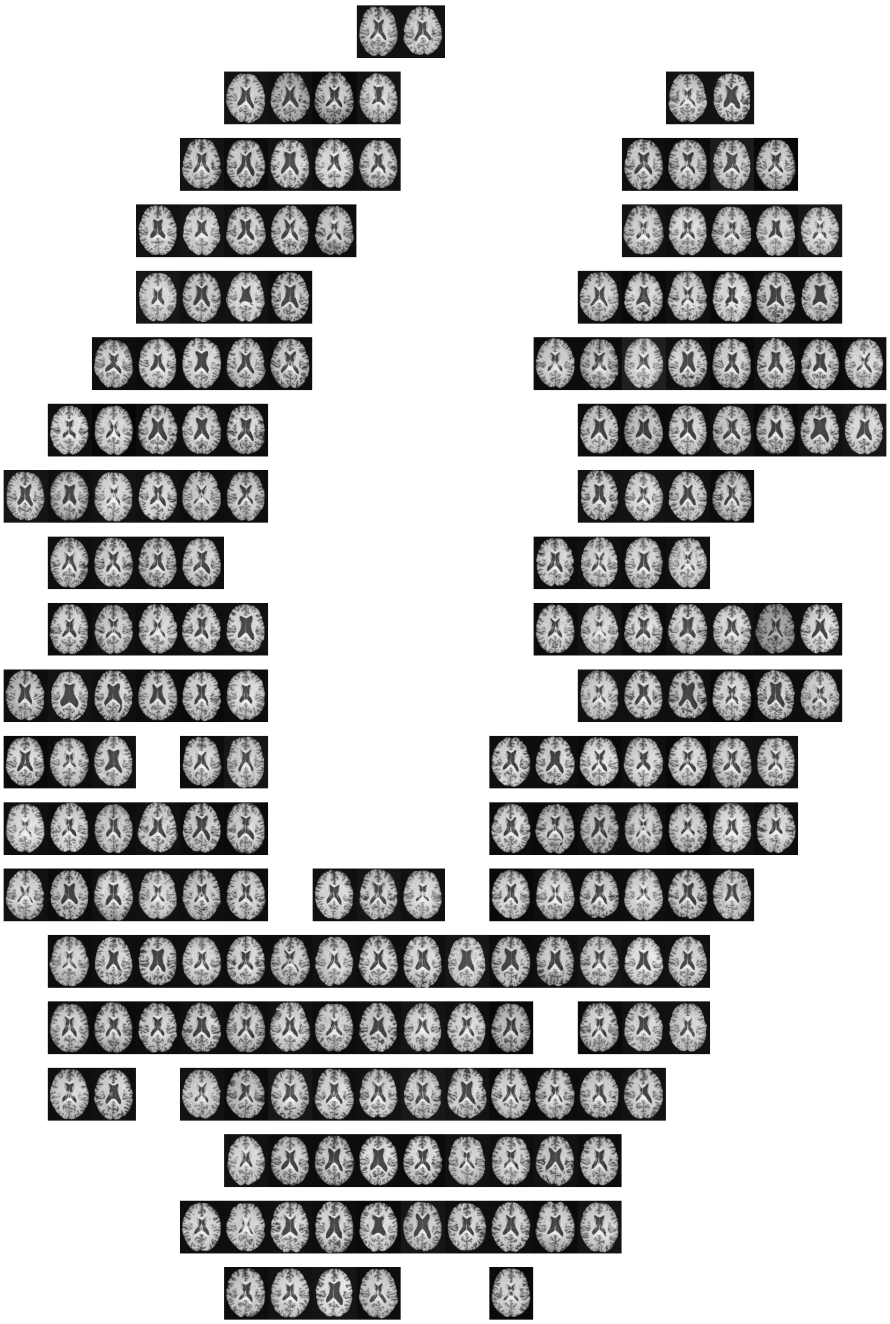

Figure 3.2: Illustration of t-SNE plot (fig. 3.1a) with ”brain manifold”

Next, we visualize how domain shifts affect the feature extraction (see fig. 3.3). Here, we only visualize the labels which the model was trained on the UKB to predict. One can observe that in

OASIS and IXI, the spatial separation of age and sex is highly preserved (see fig. 3.3 (a,b,d,e)). In contrast, features extracted from the ABIDE data show a high degree of confusion.

It is known that the MRI patterns of aging are completely different in the sexes and across ages [44]. Similarly, sex differentiation varies across ages. This might explain the high degree of confusion in the features for ABIDE: ABIDE has an age range of $5 - 56$ compared to an age range of $44 - 82$ of the UKB (see tables 2.1 and 2.2). A model pre-trained on the UKB was trained to learn age and sex differentation patterns for subjects older than subjects in ABIDE.

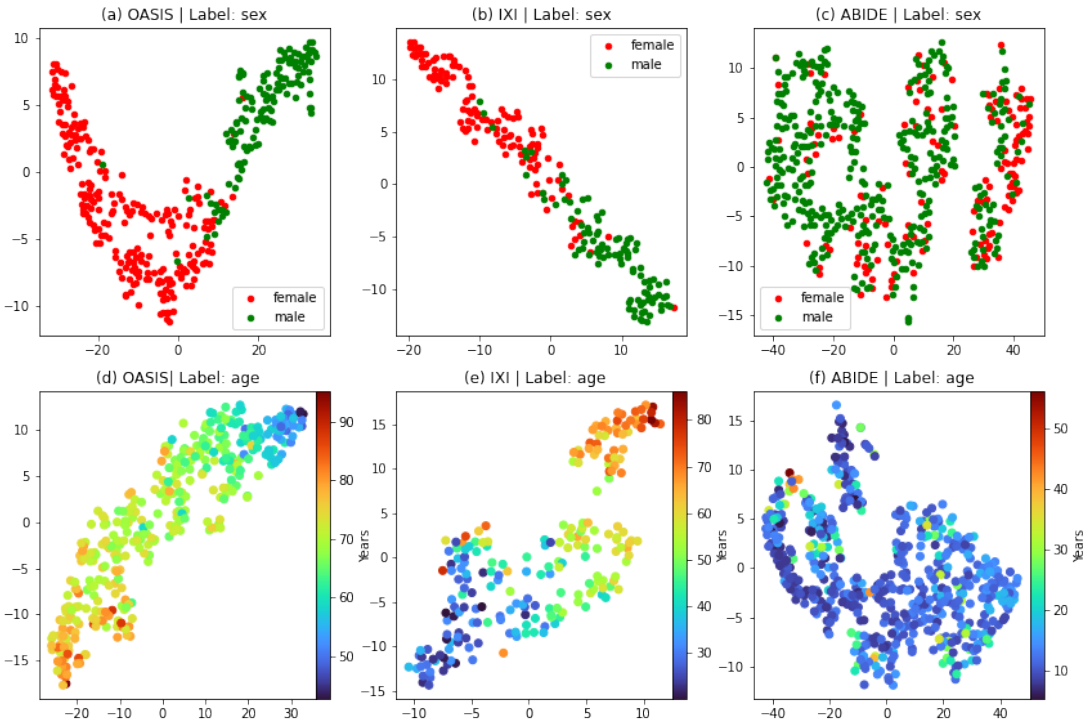

Figure 3.3: t-SNE plot of SFCN features after domain shift from UKB to various data sets. (a),(b),(c) model pre-trained on UKB sex prediction. (d),(e),(f) model pre-trained on UKB age prediction.

To quantify the effect of domain shifts on the features of a deep neural network, we fine-tune the parameters of the classifier of a pre-trained model on the target set while keeping the feature extractor constant (steps 1-9 in algorithm 1). Crucially, we use feature extractors from models pre-trained on different tasks. This allows us to evaluate how important the task is where the features were pre-trained on. In table 3.2, one can see that the models which were pre-trained on the same task outperformed models which were pre-trained on a different task. This confirms the observation from fig. 3.1 that features are task-specific. Moreover, the highly accurate results confirm the observation from fig. 3.3 that features can be highly re-usable across data sets if they

are from the same task.

Table 3.2: Results on age or sex prediction on OASIS by fine-tuning the classifier of models which were pre-trained on the UKB on age or sex prediction (mean and std over 5 runs). For sex prediction, the data sets were balanced for sex. ”MAE” is mean absolute error. ”Acc.” is accuracy.

Pre-trained (UKB)	**Task (OASIS)**	**Results**
Age	Age	3.52 ± 0.02 (MAE)
Sex	Age	6.91 ± 0.01 (MAE)
Sex	Sex	$94.6\% \pm 0.2\%$ (acc.)
Age	Sex	$52.0\% \pm 0.5\%$ (acc.)

3.1.3 Feature fine-tuning

So far, we have shown that steps 1-9 in algorithm 1 significantly improve performance. We finally study to which extent it is beneficial for model performance to perform step 10, i.e. to fine-tune the feature extractor. In principle, there should be no decrease in performance since picking a learning rate $\lambda = 0$ would simply mean leaving out this step. However, it is possible to overfit by picking hyperparameters optimizing results on the validation set.

In table 3.3, we compare the results between the full algorithm or fine-tuning only the classifier. As one would expect, we see a consistent improvement in performance on the validation set for all data sets apart from ABIDE for sex prediction. However, the test results are less clear. While we can see some overfitting in OASIS sex prediction and IXI age prediction, fine-tuning the full model usually improves results. In particular, we can see a particular big improvement for ABIDE. This fits to observation from fig. 3.3 showing a high confusion of features for ABIDE making feature fine-tuning more necessary as opposed to OASIS where features are more ordered from the start and overfitting is more prominent. In fig. 3.4, we visualize the change of feature extraction applying algorithm 1 for ABIDE age prediction and OASIS age prediction. As one would expect from the results of table 3.3, one can see a clear evolution of an age spectrum for ABIDE, while OASIS features only change little since the already separated the ages from the start.

Together, this section shows that algorithm 1 successfully exploits the re-use of deep neural networks across data sets and represents a sensible transfer learning pipeline for neuroimaging.

Table 3.3: Comparing results between fine-tuning the classifier and algorithm 1. For sex prediction, the data sets were balanced for sex. "MAE" is mean absolute error. "Acc." is accuracy. "Valid" refers to results on the validation set, "test" to results on the test set.

Data	Task	Method	Results (valid)	Results (test)
OASIS	Age	ft. class	2.96 ± 0.05 (MAE)	3.52 ± 0.02 (MAE)
		algorithm 1	2.82 ± 0.05 (MAE)	3.25 ± 0.02 (MAE)
OASIS	Sex	ft. class	$90.8\% \pm 0.7\%$ (acc.)	$94.6\% \pm 0.2\%$ (acc.)
		algorithm 1	$97.0\% \pm 1.6\%$ (acc.)	$92.6\% \pm 1.8\%$ (acc.)
IXI	Age	ft. class	6.12 ± 0.07 (MAE)	5.35 ± 0.10 (MAE)
		algorithm 1	5.82 ± 0.59 (MAE)	5.65 ± 0.55 (MAE)
IXI	Sex	ft. class	$80.0\% \pm 0.4\%$ (acc.)	$87.6\% \pm 0.3\%$ (acc.)
		algorithm 1	$85.6\% \pm 2.6\%$ (acc.)	$90.3\% \pm 1.3\%$ (acc.)
ABIDE	Age	ft. class	4.39 ± 0.21 (MAE)	4.43 ± 0.22 (MAE)
		algorithm 1	1.72 ± 0.06 (MAE)	1.70 ± 0.07 (MAE)
ABIDE	Sex	ft. class	$74.4\% \pm 0.6\%$ (acc.)	$70.2\% \pm 2.3\%$ (acc.)
		algorithm 1	$69.7\% \pm 5.4\%$ (acc.)	$75.7\% \pm 4.5\%$ (acc.)

3.2 Transfer learning vs. classical regression methods

We also compare our transfer learning pipeline (algorithm 1) with a classical regression method as described in section 2.3. Our results in table 3.4 show that the transfer learning pipeline outperforms regression methods across data sets and across tasks by a large margin. For age prediction, the mean absolute error (MAE) is approximately halfed by using transfer learning compared to elastic net regression. For sex prediction, the difference of the accuracy to 50% (i.e. random selection) is doubled for transfer learning compared to regression.

3.3 Comparing results to other works

In general, it is difficult to compare prediction results to previous works: train, validation, and test sets have different sizes and different choice of modalities and pre-processing methods might affect performance. However, we name a few to put our results into context.

For OASIS, Dinsdale et al. [45] perform age prediction on OASIS with a training size of 813 (compared to 355 here). We improve their result of 3.79 MAE to 3.25 MAE, although we use less training data.

Jónsson et al. [46] use IXI for age prediction. They link the the difference between predicted and actual gene with two genomic sequence variants correlating with reduced sulcal width and

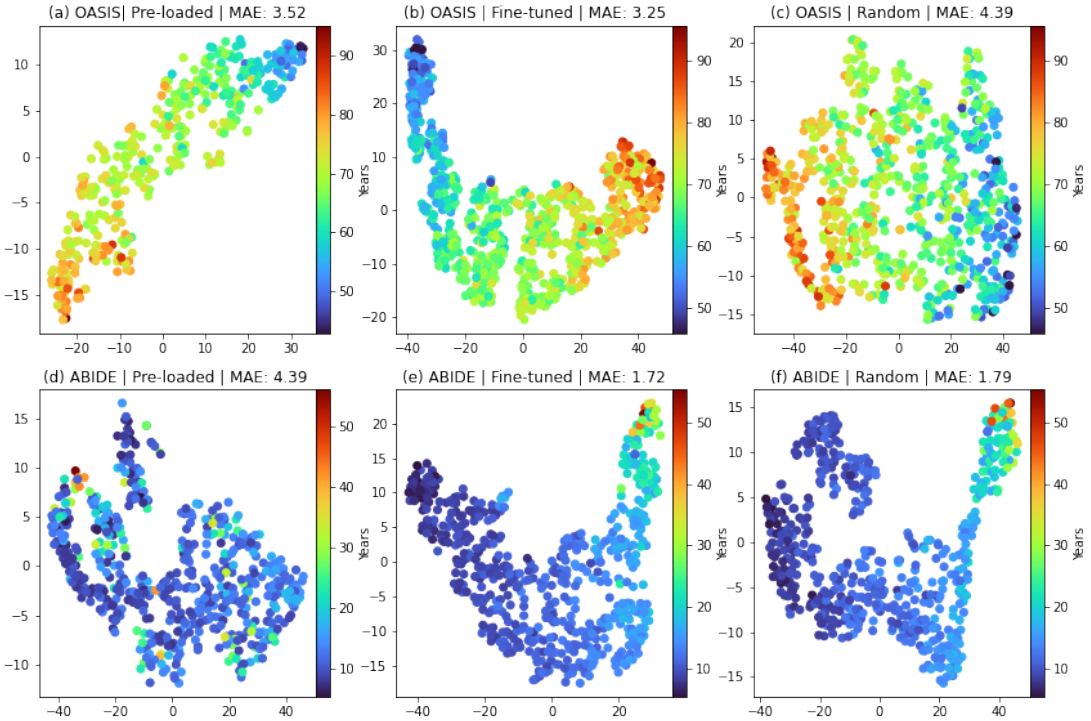

Figure 3.4: Plotting SFCN features after fine-tuning the feature extractor and training a model from scratch. (a,b) Features of OASIS/ABIDE (test set) based on UKB age prediction model. (b,d) After fine-tuning the feature extractor on OASIS/ABIDE (train set). (c,f) Features of ABIDE (test set) based on UKB age prediction model. For OASIS, the features are re-usable (a), improve by fine-tuning (b) and are not reproducible by training from scratch (c). For ABIDE, pre-trained features are not useful (d) and only fine-tuning the feature extractor brings performance gains (e), while training from scratch can create similar features (f).

reduced white matter surface area. Their result on IXI is 4.149 MAE compared to $5.$ in our work. However, the size of their training data set is 440 compared to 215 in this work. Most importantly, they used IXI for *validation*, i.e. they optimized hyperparameters on IXI and they did not report a test result on IXI. Therefore, a fair comparison to our work is not possible.

For ABIDE, Bellantuono et al. [37] achieve an MAE of 2.19 on ABIDE age prediction (compared to 1.72 here) using a larger test set and excluding 22 subjects older than 40. Our method therefore clearly improves state-of-the-art results on ABIDE age prediction.

Table 3.4: Comparing elastic net regression (see section 2.3) with transfer learning (see algorithm 1). For age prediction, naive prediction is prediction of the mean of the training set. For sex prediction, it is random selection. For sex prediction, the data sets were balanced for sex.

Dataset	**Method**	**Age**	**Sex**
OASIS	Naive	6.94 ± 0.00	$50.0\% \pm 0.0\%$
	Elastic	6.24 ± 0.52	$67.0\% \pm 3.9\%$
	Algorithm 1	3.25 ± 0.02	$92.6\% \pm 1.8\%$
IXI	Naive	13.16 ± 0.00	$50.0\% \pm 0.0\%$
	Elastic	9.90 ± 0.26	$73.1\% \pm 4.7\%$
	Algorithm 1	5.65 ± 0.55	$90.3\% \pm 1.3\%$
ABIDE	Naive	4.12 ± 0.00	$50.0\% \pm 0.0\%$
	Elastic	3.59 ± 0.60	$66.9\% \pm 1.8\%$
	Algorithm 1	1.70 ± 0.07	$75.7\% \pm 4.5\%$

3.4 Explaining the performance gain of transfer learning

To study the high performance of transfer learning, we next compare our method with training a model from scratch, i.e. randomly initialize the weights and biases of the network instead of loading them from a pre-trained model. As one can see in table 3.5, transfer learning outperforms training from scratch in all cases apart from ABIDE sex prediction. As one might expect from fig. 3.3, the pre-trained features for ABIDE sex prediction are not useful and even lead to worse results than training from scratch. This phenomenon is called *negative transfer* which refers to less accuracy due to transfer learning mainly caused by the source and target domain not related ”enough” [47]. In the context of MR brain imaging, this has already been observed to lead to worse results [48].

In previous works, it was claimed that the performance gain of transfer learning can mainly be attributed to the correct scaling of parameters of the networks as opposed to actual re-use of features [21]. To test this, we compare the performance of transfer learning with the following method of random initialization of weights: every layer is randomly initialized with mean and variance given by the mean and variance of the weights of a pre-loaded model. Crucially, we use algorithm 1 to train this model (not training from scratch). The results in table 3.5 show that this scaled random initialization does not show a performance comparable to algorithm 1. This shows that it is the actual feature transfer or feature re-use which explains the boost in performance due to transfer learning.

Overall, the results in table 3.5 show that it is not merely using a deep neural network but transfer learning which brings meaningful performance gains.

Table 3.5: Comparing transfer learning with random initialization of parameters of the network. ”Random” denotes training from random initialization via classical SGD. Algorithm 1 (Re-init) follows algorithm 1 but before step 4 randomly re-intializes every layer of the model M with mean and variances given by the pre-trained parameters.

Dataset	**Method**	**Age**	**Sex**
OASIS	Random	4.39 ± 0.10	$80.9\% \pm 3.1\%$
	Algorithm 1 (Re-init)	5.28 ± 0.20	$86.3\% \pm 2.0\%$
	Algorithm 1	3.25 ± 0.02	$92.6\% \pm 1.8\%$
IXI	Random	6.24 ± 0.15	$71.2\% \pm 5.6\%$
	Algorithm 1 (Re-init)	7.11 ± 0.63	$86.9\% \pm 2.8\%$
	Algorithm 1	5.65 ± 0.55	$90.3\% \pm 1.3\%$
ABIDE	Random	1.79 ± 0.04	$79.6\% \pm 2.6\%$
	Algorithm 1 (Re-init)	2.04 ± 0.21	$64.1\% \pm 7.6\%$
	Algorithm 1	1.70 ± 0.07	$75.7\% \pm 4.5\%$

3.5 Transfer learning and data scarcity

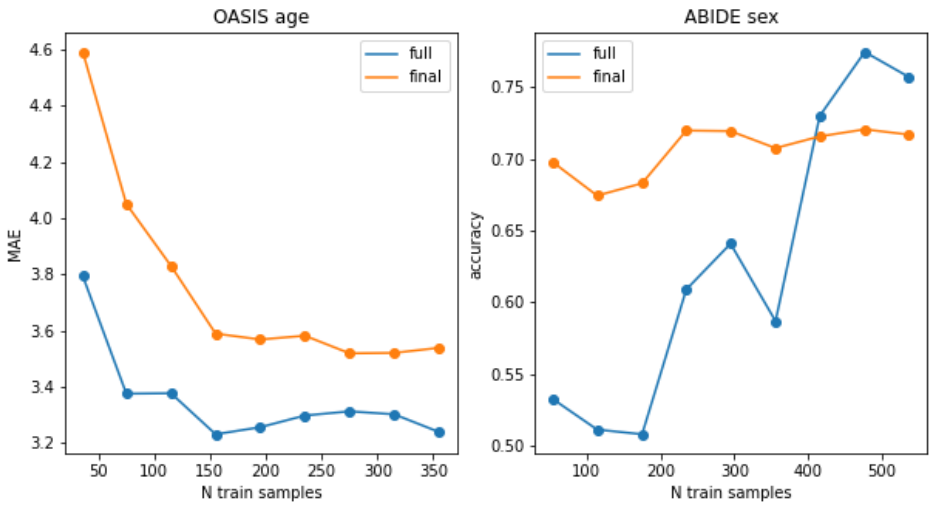

Figure 3.5: Studying performance depending on the size of the training set. ’full’ refers to the full transfer learning method (algorithm 1), and ’final’ for fine-tuning only the final layer. Left: OASIS age prediction. Right: ABIDE sex prediction.

The scarcity of data is one of the main challenges in applying deep learning to neuroimaging. For a successful application of our transfer learning pipeline, it is therefore crucial how many data samples are needed to improve accuracy. We study this here. Beyond the transfer learning pipeline, we also test fine-tuning only the classifier (i.e. final layer) of the model. We do experiments varying the size of the training set keeping the size of the test set constant.

In fig. 3.5, we can see that for OASIS age prediction, the full transfer learning algorithm gives very accurate results even for as few training samples as 50. It also consistently outperforms fine-tuning only the final layer. In contrast, for ABIDE sex prediction, we observe that algorithm 1 is only better if the number of training samples is higher than 400. With too few samples, we observe that the full transfer learning pipeline overfits to the small training set. Therefore, only fine-tuning the final layer might be a more sensible choice in the very small data regime.

3.6 Convergence time

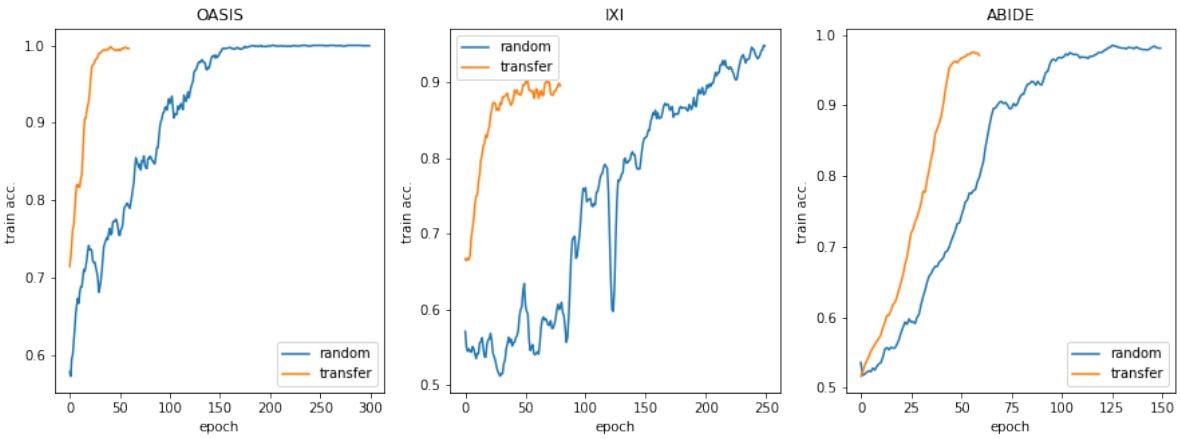

Figure 3.6: Comparing training convergence between randomly initialized models and transfer learning. One can see that the training accuracy improves much quicker and flattens much faster for a pre-trained model.

Beyond performance accuracy, there are other practical advantages which transfer learning might bring. Intuitively, a pre-trained model has a "headstart" and needs less training iterations. We study this for sex prediction on OASIS, IXI, and ABIDE.[1] In fig. 3.6, we can indeed observe a stronger convergence. Even in cases where the performance gain of transfer learning is

[1] A fair comparison for age prediction would be difficult. As outlined in algorithm 1, the transfer learning process has two steps in this case (fine-tuning classifier+full model), while training from scratch has only one.

minor such as for ABIDE, one can observe a clear speed-up of training due to transfer learning. Hence, transfer learning is beneficial not only for performance but also for training efficiency.

4 Discussion

4.1 Pre-training on large data sets

In this work, we showed that ”simple” transfer learning leads to performance improvements for neuroimaging as it does for natural image data sets. This is particularly interesting when comparing our work to Raghu et al. [21], who argue that fine-tuning pre-training models does not bring any performance gains in biomedical imaging. However, our work is consistent with their results since we use a neuroimaging data set for pre-training as opposed to a natural image data set. In section 3.1.2, we have shown that features which a neural network learns from data are very specific to the neuroimaging domain, even specific to the tasks such as age and sex. Similarly, visualizations of convolutional kernels trained on ImageNet have been shown to lead to features that are suited for detecting natural images [49]. As Raghu et al. [21] also remarked, it therefore seems plausible that pre-training on a natural image data set such as ImageNet does not bring any performance gains in the biomedical domain beyond favourable initial scaling of the weights, while data sets such as the UKB do.

In computer vision, the discovery that features learned on a pre-training task can be useful to a target task [50, 49] have led to the following practice: initial pre-training models on ImageNet with subsequent fine-tuning on the target task. From a computer vision perspective, we showed in this work that the UKB can serve as the ”ImageNet” for neuroimaging, i.e. the UKB can provide a training task for a deep neural network which is ”similar enough” to the task of interest. While we used the currently available ~ 40000 samples, the UKB continues to grow in size to 100000 in the next years [22]. Its power to enable effective and simple transfer learning is therefore likely to grow as well.

However, there are certain challenges. In neuroimaging, technical variations have been observed to be a much more significant problem than for natural images and the UKB does not cover the whole spectrum of MRI scanners, image protocols, etc. (see table 2.2). More importantly, since the UKB is not disease-specific, it is difficult to pre-train a model on disease prediction. Given the results in table 3.2, it therefore remains an open question how to transfer across tasks and how to use the UKB for direct disease prediction as opposed to biomarkers such as the brain age delta.

4.2 Traditional machine learning vs. deep learning

While the advantages of deep learning above regression methods have been a subject of debate, recent work showed that deep learning outperforms traditional regression methods on age and

sex prediction on UKB [24].

Considering that our method mainly relies on re-training the classifier, it can be considered as a regression method based on features previously learnt from a big neuroimaging data sets. Therefore, the claim that regression methods outperform deep learning on small data sets might still be true - we simply use more informative features. This is particular striking given results in fig. 3.5 which show that fine-tuning the final layer (pure regression on the features) can outperform the full transfer learning method if there are only few data samples available.

However, comparing table 3.4 and table 3.5 we observe that even random initialization outperforms regression methods. Therefore, our work shows that the superior performance of deep learning also applies to the small data regime - without but even more significantly with transfer learning.

4.3 Transfer learning vs. training from scratch

For natural images and computer vision, He et al. [51] challenge the assumption that pre-training on ImageNet brings performance gains beyond training from scratch. They report similar results of transferred and randomly initialized models. However, they find that transfer learning leads to faster convergence. In this work, we also show that transfer learning speeds up convergence. But in contrast, we show that for neuroimaging transfer learning actually brings performance gains in terms of accuracy.

4.4 Comparison with other transfer learning approaches

4.4.1 Feature-based approaches

While our transfer learning method also fine-tunes the full model, we showed that the main performance gains come from fine-tuning the classifier, i.e. the parameters of the final layer of our network, for every target data set (see table 3.3). However, other works are more ”feature-based” in the sense that transfer learning happens on a feature level - for SFCNs this would be the feature extractor (see fig. 2.1).

Symmetric feature-based approaches harmonize features from the source and target domain. For example, Dinsdale et al. [45] proposed a method based on adversarial training unlearning information about the scanner sites enabling multi-scanner integration and generalization with a *single* classifier across data sets. Other works performed such an harmonization on the feature level by minimizing their distances via different metrics such as mutual information [52] or maximizing their correlation [53, 54]. The results of this work show that a harmonization on the feature level is not necessarily needed if the differences across data sets are small (e.g. OASIS and UKB, see fig. 3.3 and table 2.2). However, it is interesting that the ”most inhomogeneous” data set, i.e. ABIDE with its big variety of scanner models used (see table 2.2), led to the

worst results for us. Therefore, the need for harmonizing different data sets on a feature level seems to remain and it would be interesting to study a combination of a ”feature-based” and a ”classifier-based” approach.

4.4.2 Style transfer approaches

A further approach to alleviate the problem of domain shift is using style transfer methods. Such methods allow to transfer an MRI scan of ”style A”, e.g. the image properties of MRI scanner A, to ”style B”, e.g. the image properties of MRI scanner B [55]. Ali et al. [56] propose a transfer learning method based on Generative Adversarial Network (CycleGAN) [57] to transfer images across different sites and provide promising results. Similarly, Bashyam et al. [58] use CycleGANs to map MRI data from different data sets to a canonical reference domain where the image appearance does not depend on the scanner site.

A style-transfer approach could also extend our transfer learning method: instead of using the UKB for pre-training (step 3 in algorithm 1), one could create an OASIS-style UKB (resp. ABIDE-style, IXI-style UKB) via CycleGANs and use it for pre-training. Subsequently, one could continue with algorithm 1 as above. Future work could explore whether such an approach improves results. In this work, we focused on using simple methods since these promise to be of greatest use in the clinic.

4.4.3 Instance-based approaches

Another possibility to solve the problem of domain shift is to take an *instance*-based approach where similarities at the MR images themselves are modelled to transfer knowledge. For example, previous work weighted test images based on the similarity to the training images and classifying via weighted Support Vector Machines (SVMs) [59]. Cheng et al. [60] performed a similar analysis with combined feature selection and sample selection. Unfortunately, in our case such an approach would mean re-training the model for every test which is impractical with deep learning methods and the current computational power.

4.4.4 Methods different from transfer learning

There are various related strategies to transfer learning: first, meta-learning algorithms *train* models to learn from less data. For example, Liu et al. [61] showed that model-agnostic meta-learning [62] can lead to highly accurate results in MR prostate images. However, meta-learning optimizes to obtain a convergence of the *training* process within a few steps - only indirectly influencing the number of required data points. In general, the number of epochs needed to obtain convergence of the training process is not of particular importance in biomedical imaging if it is not excessively big. In this work, we also showed that even in cases where transfer learning does not bring a big performance gain, it can still speed up training significantly (see fig. 3.6). Therefore, the actual benefit of meta-learning approaches compared to our approach remain unclear.

Second, multi-task learning algorithms are machine learning methods that can perform several tasks at the same time. These were also successfully applied to brain and tumor segmentation [63, 64]. For our purposes, this could mean pre-training a SFCN on age and sex prediction at the same time. It would then be interesting to re-plot the features as in fig. 2.1 and see whether features are now less task-specific. In this case, a transfer across tasks, even to disease prediction, might indeed be possible.

5 Conclusion

In this work, we proposed a transfer learning method based on the re-use of deep neural network features to alleviate the problem of domain shift across different MRI scanner sites and data sets. We showed that the performance gain can be attributed to the re-use of features across data sets. Our method achieved state-of-the-art results on age and sex prediction and led to more efficient training. Future work could combine the method with other transfer learning approaches to enable transfer to novel tasks such as disease prediction. In sum, transfer learning via re-use of deep neural network features might therefore provide a simple and efficient way of achieving highly accurate results in neuroimaging as necessary to apply deep learning in the clinic.

Bibliography

[1] Russakovsky, O. et al. (2015) Imagenet large scale visual recognition challenge. International journal of computer vision, 115, 211–252

[2] LeCun, Y. et al. (2015) Deep learning. nature, 521, 436–444

[3] Hirschberg, J. and Manning, C.D. (2015) Advances in natural language processing. Science, 349, 261–266

[4] Hinton, G. et al. (2012) Deep neural networks for acoustic modeling in speech recognition: The shared views of four research groups. IEEE Signal processing magazine, 29, 82–97

[5] Cheng, J.Z. et al. (2016) Computer-aided diagnosis with deep learning architecture: applications to breast lesions in us images and pulmonary nodules in ct scans. Scientific reports, 6, 1–13

[6] Cicero, M. et al. (2017) Training and validating a deep convolutional neural network for computer-aided detection and classification of abnormalities on frontal chest radiographs. Investigative radiology, 52, 281–287

[7] Kooi, T. et al. (2017) Large scale deep learning for computer aided detection of mammographic lesions. Medical image analysis, 35, 303–312

[8] Ronneberger, O. et al. (2015) U-net: Convolutional networks for biomedical image segmentation. In *International Conference on Medical image computing and computer-assisted intervention*, Springer, 234–241

[9] Esteva, A. et al. (2019) A guide to deep learning in healthcare. Nature medicine, 25, 24–29

[10] He, T. et al. (2018) Do deep neural networks outperform kernel regression for functional connectivity prediction of behavior? BioRxiv, 473603

[11] He, T. et al. (2020) Deep neural networks and kernel regression achieve comparable accuracies for functional connectivity prediction of behavior and demographics. NeuroImage, 206, 116276

[12] Schulz, M.A. et al. (2019) Deep learning for brains?: Different linear and nonlinear scaling in uk biobank brain images vs. machine-learning datasets. BioRxiv, 757054

[13] Abrol, A. et al. (2021) Deep learning encodes robust discriminative neuroimaging representations to outperform standard machine learning. Nature communications, 12, 1–17

[14] Zabihi, M. et al. (2021) Non-linearity matters: a deep learning solution to generalization of hidden brain patterns across population cohorts. bioRxiv

[15] Chen, J. et al. (2014) Exploration of scanning effects in multi-site structural mri studies. Journal of neuroscience methods, 230, 37–50

[16] Castro, D.C. et al. (2020) Causality matters in medical imaging. Nature Communications, 11, 1–10

[17] Crimi, A. et al. (2018) *Brainlesion: Glioma, Multiple Sclerosis, Stroke and Traumatic Brain Injuries: Third International Workshop, BrainLes 2017, Held in Conjunction with MICCAI 2017, Quebec City, QC, Canada, September 14, 2017, Revised Selected Papers*, volume 10670. Springer

[18] Kolesnikov, A. et al. (2019) Big transfer (bit): General visual representation learning. arXiv preprint arXiv:1912.11370, 6, 8

[19] Esteva, A. et al. (2017) Dermatologist-level classification of skin cancer with deep neural networks. nature, 542, 115–118

[20] Gulshan, V. et al. (2016) Development and validation of a deep learning algorithm for detection of diabetic retinopathy in retinal fundus photographs. Jama, 316, 2402–2410

[21] Raghu, M. et al. (2019) Transfusion: Understanding transfer learning for medical imaging. arXiv preprint arXiv:1902.07208

[22] Miller, K.L. et al. (2016) Multimodal population brain imaging in the uk biobank prospective epidemiological study. Nature neuroscience, 19, 1523–1536

[23] Van Essen, D.C. et al. (2013) The wu-minn human connectome project: an overview. Neuroimage, 80, 62–79

[24] Peng, H. et al. (2021) Accurate brain age prediction with lightweight deep neural networks. Medical Image Analysis, 68, 101871

[25] LaMontagne, P.J. et al. (2019) Oasis-3: longitudinal neuroimaging, clinical, and cognitive dataset for normal aging and alzheimer disease. MedRxiv

[26] Di Martino, A. et al. (2017) Enhancing studies of the connectome in autism using the autism brain imaging data exchange ii. Scientific data, 4, 1–15

[27] (????) The IXI brain development data set. `http://https://brain-development.org/`, accessed: 2021-04-04

[28] Kaufmann, T. et al. (2019) Common brain disorders are associated with heritable patterns of apparent aging of the brain. Nature neuroscience, 22, 1617–1623

[29] Cole, J.H. et al. (2018) Brain age predicts mortality. Molecular psychiatry, 23, 1385–1392

[30] Long, J. et al. (2015) Fully convolutional networks for semantic segmentation. In *Proceedings of the IEEE conference on computer vision and pattern recognition*, 3431–3440

[31] Ioffe, S. and Szegedy, C. (2015) Batch normalization: Accelerating deep network training by reducing internal covariate shift. In *International conference on machine learning*, PMLR, 448–456

[32] Srivastava, N. et al. (2014) Dropout: a simple way to prevent neural networks from overfitting. The journal of machine learning research, 15, 1929–1958

[33] Polyak, B.T. (1964) Some methods of speeding up the convergence of iteration methods. Ussr computational mathematics and mathematical physics, 4, 1–17

[34] Paszke, A. et al. (2017) Automatic differentiation in pytorch

[35] Zhuang, F. et al. (2020) A comprehensive survey on transfer learning. Proceedings of the IEEE, 109, 43–76

[36] Alfaro-Almagro, F. et al. (2018) Image processing and quality control for the first 10,000 brain imaging datasets from uk biobank. Neuroimage, 166, 400–424

[37] Bellantuono, L. et al. (2021) Predicting brain age with complex networks: From adolescence to adulthood. Neuroimage, 225, 117458

[38] Smith, S.M. et al. (2004) Advances in functional and structural mr image analysis and implementation as fsl. Neuroimage, 23, S208–S219

[39] Jenkinson, M. et al. (2002) Improved optimization for the robust and accurate linear registration and motion correction of brain images. Neuroimage, 17, 825–841

[40] Jenkinson, M. and Smith, S. (2001) A global optimisation method for robust affine registration of brain images. Medical image analysis, 5, 143–156

[41] Greve, D.N. and Fischl, B. (2009) Accurate and robust brain image alignment using boundary-based registration. Neuroimage, 48, 63–72

[42] Zou, H. and Hastie, T. (2005) Regularization and variable selection via the elastic net. Journal of the royal statistical society: series B (statistical methodology), 67, 301–320

[43] Van der Maaten, L. and Hinton, G. (2008) Visualizing data using t-sne. Journal of machine learning research, 9

[44] Smith, S.M. et al. (2020) Brain aging comprises many modes of structural and functional change with distinct genetic and biophysical associations. Elife, 9, e52677

[45] Dinsdale, N.K. et al. (2021) Deep learning-based unlearning of dataset bias for mri harmonisation and confound removal. NeuroImage, 228, 117689

[46] Jónsson, B.A. et al. (2019) Brain age prediction using deep learning uncovers associated sequence variants. Nature communications, 10, 1–10

[47] Wang, Z. et al. (2019) Characterizing and avoiding negative transfer. In *Proceedings of the IEEE/CVF Conference on Computer Vision and Pattern Recognition*, 11293–11302

[48] Leen, G. et al. (2012) Focused multi-task learning in a gaussian process framework. Machine learning, 89, 157–182

[49] Zeiler, M.D. and Fergus, R. (2014) Visualizing and understanding convolutional networks. In *European conference on computer vision*, Springer, 818–833

[50] Girshick, R. et al. (2014) Rich feature hierarchies for accurate object detection and semantic segmentation. In *Proceedings of the IEEE conference on computer vision and pattern recognition*, 580–587

[51] He, K. et al. (2019) Rethinking imagenet pre-training. In *Proceedings of the IEEE/CVF International Conference on Computer Vision*, 4918–4927

[52] Mansoor, A. and Linguraru, M.G. (2019) Communal domain learning for registration in drifted image spaces. In *International Workshop on Machine Learning in Medical Imaging*, Springer, 479–488

[53] Cai, X.L. et al. (2020) Generalizability of machine learning for classification of schizophrenia based on resting-state functional mri data. Human brain mapping, 41, 172–184

[54] Guerrero, R. et al. (2014) Manifold alignment and transfer learning for classification of alzheimer's disease. In *International Workshop on Machine Learning in Medical Imaging*, Springer, 77–84

[55] Tokuoka, Y. et al. (2019) An inductive transfer learning approach using cycle-consistent adversarial domain adaptation with application to brain tumor segmentation. In *Proceedings of the 2019 6th International Conference on Biomedical and Bioinformatics Engineering*, 44–48

[56] Ali, M.B. et al. (2020) Domain mapping and deep learning from multiple mri clinical datasets for prediction of molecular subtypes in low grade gliomas. Brain Sciences, 10, 463

[57] Zhu, J.Y. et al. (2017) Unpaired image-to-image translation using cycle-consistent adversarial networks. In *Proceedings of the IEEE international conference on computer vision*, 2223–2232

[58] Bashyam, V.M. et al. (2020) Medical image harmonization using deep learning based canonical mapping: Toward robust and generalizable learning in imaging. arXiv preprint arXiv:2010.05355

[59] van Opbroek, A. et al. (2015) Weighting training images by maximizing distribution similarity for supervised segmentation across scanners. Medical image analysis, 24, 245–254

[60] Cheng, B. et al. (2015) Domain transfer learning for mci conversion prediction. IEEE Transactions on Biomedical Engineering, 62, 1805–1817

[61] Liu, Q. et al. (2020) Shape-aware meta-learning for generalizing prostate mri segmentation to unseen domains. In *International Conference on Medical Image Computing and Computer-Assisted Intervention*, Springer, 475–485

[62] Finn, C. et al. (2017) Model-agnostic meta-learning for fast adaptation of deep networks. In *International Conference on Machine Learning*, PMLR, 1126–1135

[63] Weninger, L. et al. (2019) Multi-task learning for brain tumor segmentation. In *International MICCAI Brainlesion Workshop*, Springer, 327–337

[64] Zhou, C. et al. (2020) One-pass multi-task networks with cross-task guided attention for brain tumor segmentation. IEEE Transactions on Image Processing, 29, 4516–4529